Acta Mechanica Sinica
https://doi.org/10.1007/s10409-020-00996-7

RESEARCH PAPER

Assessment of the potential storm tide inundation hazard under climate change: case studies of Southeast China coast

Bingchuan Nie[1,2] · Qingyong Wuxi[3,4] · Jiachun Li[3,4] · Feng Xu[1,2]

Received: 4 March 2020 / Revised: 28 May 2020 / Accepted: 29 June 2020
© The Chinese Society of Theoretical and Applied Mechanics and Springer-Verlag GmbH Germany, part of Springer Nature 2020

Abstract
Four typical cases of storm tide inundation at one of the typical storm surge prone areas in China and worldwide, i.e. Southeast China coast, are presented to demostrate the impact of climate change. It is relied on the statistical trend analysis of tropical cyclone intensification (TCI) and sea level rise (SLR) considering temporally non-stationary and spatially non-uniform effects, numerical analysis taking into account the tide-surge-wave coupling effect and GIS-based analysis for inundation evaluation. The results show that the high sea surface elevation tends to occur in the bays and around the estuaries. The maximal sea surface elevations of the worst situation at present without considering TCI and SLR (i.e. scenario S2) are 6.06 m, 5.82 m and 5.67 m around Aojiang, Feiyunjiang and Oujiang river estuaries, respectively. Whereas, the maximal sea surface elevations for the three estuaries would increase to 7.02 m, 6.67 m and 6.44 m, respectively, when the non-stationary extreme wind speed of 100-year recurrence period and SLR equivalent to the situation of 2100s (i.e. scenario S4) are taking into account. The potential inundation area of scenario S4 would expand by 108% to about 798 km^2 compared with scenario S2. In addition, the remotely sensed maps and inundation durations of the hardest hit regions are provided, which will aid the prevention and mitigation of storm tide inundation hazard and future coastal management there.

Keywords Storm surge · Inundation · Risk assessment · Tropical cyclone intensification · Sea level rise

1 Introduction

Storm surge caused by tropical cyclone (TC) is one of the most hazardous events for coastal zones. Superimposing over the astronomical tide, it has produced devastating damage in low-lying areas worldwide in history [1]. Although the operational forecast of storm tide (nonlinear superposition of storm surge and astronomical tide) has made a great progress in the past decades, a few individual disastrous storm events still caused extensive damages recently, say, TC Haiyan in 2013 resulted in 6300 dead and 1061 missing in Philippines alone [2].

Inundation is one of the most catastrophic consequences in a storm tide event. To reduce the potential losses during inundation, risk assessment is an effective and practical way out. Based on the surge response function, which gives the relations between maximum surge elevations and hurricane parameters, Hsu et al. [3] examined the risk of northern Gulf of Mexico coast exposed to storm surge. Christie et al. [4] investigated the coastal flood risk in North Norfolk, in which CS3X Continental Shelf tidal surge model and 1D SWAN model are adopted. Younus [5] carried out the risk assessment of storm tide with focus on the vulnerability. Fifty-six vulnerability issues are identified, and their categories and weighted index scale are provided. Taflanidis et al. [6] carried out the risk estimation of TC waves, sea surface elevations, and run-up for TC passing by the Island of Oahu. In their work, a response surface methodology fed by information from precomputed database is adopted to evaluate the maximum wave height and water level according to the hurricane parameters. In those works, risk assessment is usually divided into hazard and vulnerability assessments. The

✉ Jiachun Li
jcli08@imech.ac.cn

1 School of Civil Engineering, Beijing Jiaotong University, Beijing 100044, China

2 Beijing's Key Laboratory of Structural Wind Engineering and Urban Wind Environment, Beijing 100044, China

3 Key Laboratory for Mechanics in Fluid Solid Coupling Systems, Institute of Mechanics, Chinese Academy of Sciences, Beijing 100190, China

4 School of Engineering Science, University of Chinese Academy of Sciences, Beijing 100049, China

Published online: 25 November 2020

vulnerability assessment is devoted to figure out the resistant capability of coastal zones towards storm tide inundation. While, the hazard assessment, the prerequisite of vulnerability assessment, is aimed to evaluate the natural attributes (intensity and frequency) of storm tide inundation. In general, the hazard assessments in the aforementioned works remain to be improved: (1) the precisions of models for sea surface elevation predicting are unsatisfactory, and (2) the intensity of storm tide inundation including area, depth and duration needs to be comprehensively quantified.

Many researchers were devoted to developing hydrodynamic models with good precision and high performance for storm tide prediction. Jelesnianski et al. [7] built the popular SLOSH model which is still extensively used in operational forecast of storm surge. The ADCIRC model developed by Luettich and his colleagues [8], which has been improved continuously, is widely applied in the academic and engineering communities. Other hydrodynamic models such as POM, ROMS, ELCIRC, FVCOM, SELFE and CH3D have been used for storm surge studies as well. The aforementioned hydrodynamic storm surge models have been further upgraded to couple with the wave models recently. The typical works are: the ADCIRC+SWAN model [9,10], the FVCOM-SWAVE model [11] and the SELFE-WWM-II model [12]. Based on those coupled models, the surge-tide-wave coupling effects can be readily presented. Zhang et al. [13] concluded that the deviation of sea surface elevation of order of one meter can be caused owing to nonlinear tide-surge interaction. Wuxi [14] observed wave induced surge and tide-surge interaction along Zhe-Min coast. They found that the relative error of sea surface elevation due to tide-surge coupling effect can be as high as 28%. These facts imply that the surge-tide-wave coupled models are preferred in the hazard assessment of storm tide inundation (not common at present).

Besides the precision of hydrodynamic model, the challenging issues due to climate change, scarely discussed in the previous hazard assessment, needs more attention. Tropical cyclone intensification (TCI) and sea level rise (SLR) are the most obvious ones among the direct influential factors. Webster et al. [15] examined the intensity of TC, they pointed out that TCs in the strongest Saffir-Simpson categories 4 and 5 have almost doubled in both number and proportion in the period 1970–2004 for all ocean basins. Relied on the satellite-based estimation of TC intensity, Elsner et al. [16] reported that significant wind speed upward trends of 0.30 ± 0.09 m/s per year can be observed for the strongest TCs. The study by Knutson et al. [17] shows that the globally averaged intensity of TC could increase 2–11% by 2100 due to greenhouse warming. Recently, Wang [18] examined the extreme wind speeds in Northwest Pacific Ocean (NWP) and South China Sea (SCS), and announced that the spatial inhomogeneous and non-stationary effects should be considered. As for the SLR, the AR5 of IPCC predicted the future global SLR under representative concentration pathway (RCP) 2.6, RCP 4.5, RCP 6.0, and RCP 8.5 [19]. They also claimed about 70% of the coastlines worldwide would experience lower SLR than the global mean SLR by 2100s. Those results demonstrate that both TCI and SLR have significant spatial inhomogeneous and non-stationary effects.

Recently, the impacts of TCI and SLR on coastal hazard in a few regions have been investigated preliminarily. Feng et al. [20] examined the storm surge trends in the coastal areas of China from 1997 to 2016. They concluded that the increasing rate of extreme storm surge is as high as 0.06 m per year at 90% confidence level. However, the impact of future SLR on inundation is out of consideration. Wang [21] simulated the inundation in Shanghai considering SLR, land subsidence. They found that 46% of the seawalls and levees are projected to be overtopped by 2100. Feng et al. [22] investigated the inundation risk of extreme sea surface elevations in Rongcheng based on the Pearson Type III distribution considering gobal SLR under situations RCPs 2.6, 4.5 and 8.5, which implies the spatial inhomogeneous effect of SLR is neglected. The influences of TCI are not examined in the aforementioned two works either. Yin [23] studied the impacts of SLR and TCI, which are artificially designed, on storm surges and waves at Pearl River Estuary. Li et al. [24] studied the coastal flood hazards at Oahu for 24 TCs in 2080-2099 by the CMIP5 NCAR-CCSM4 model and the SLR under RCP 8.5. In general, the impacts of TCI and SLR are scarcely considered at present with focus on the risk assessment of storm tide inundation. In a few relevant works available, TCI or SLR usually are artificially given or obtained according to the existing global averaged results, which means the spatial inhomogeneous and non-stationary effects are neglected. Moreover, considering the significant regional differences, impacts of TCI and SLR on the storm tide inundation at typical storm surge prone areas remain to be carried out as well.

Motivated by the aforementioned facts, a methodology for long-term hazard assessment of storm tide inundation is implemented in this work. It integrates the statistical trend analysis considering temporally non-stationary and spatially non-uniform effects, numerical analysis taking into account the tide-surge-wave coupling effect and GIS-based analysis for inundation evaluation. Based on that, scenario analysis is presented for Southeast China coast.

Southeast China coast is one of the typical storm surge prone areas in China and worldwide along the west coast of oceans from the view of intensity and occurrence frequency of TC and the damages caused. According to the annual report of national marine hazard issued in 1990-2018 by Ministry of Natural Resource of China, the annual average direct economic loss caused by storm tide in China is about 1.73 billion USD, and no downtrend can be observed

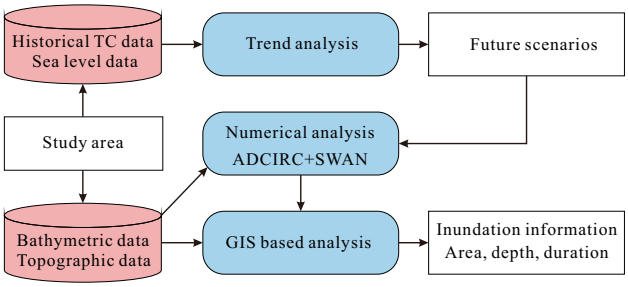

Fig. 1 Flow chart for hazard assessment of storm tide inundation. The red cylinders and blue rounded rectangles represent the data sets and analytical approaches, respectively

over the last three decades. Moreover, TCs make landfall at Southeast China coast tend to have stronger intensity than the other places. The literature review shows that inundation caused by storm tide there is scarcely studied, let alone the long-term hazard assessment of storm tide inundation considering potential TCI and SLR. The corresponding results can provide reference for the local prevention and mitigation of storm tide inundation hazard and future coastal management.

2 Methodology

The main steps of hazard assessment of storm tide inundation considering TCI and SLR are summarized by the flow chart in Fig. 1. The details of the trend analysis, numerical analysis and GIS-based analysis are described as below.

2.1 Statistical analysis of SLR and TCI

TCI and SLR are the most direct influential factors for long-term hazard assessment of storm tide inundation. Numerous results about global mean TCI and SLR are available in literatures, e.g. Refs. [16,17]. However, using those results directly would introduce significant deviation for a specific study area due to the significant spatial inhomogeneous effect.

The influential factors of SLR (or TCI) are plenty and complex, and may highly related to future greenhouse gas emission control. To predict future SLR (or TCI), two solutions can be usually found in literatures. One is based on the climate models such as Coupled Model Inter-comparison Project Phase 5 (CMIP5) or the coming CMIP 6. The other one is purely data-driven prediction, i.e. estimating SLR (or TCI) based on statistically analyzing the long-term measurement of sea level. We chose the latter one because of simpler procedure.

TCI and SLR is estimated by analyzing the long-term historical data of the study area. To consider the non-stationary effect, the non-stationary extreme value theory and nonlinear fitting are adopted for the TCI and SLR, respectively. The basic conception of the non-stationary extreme value theory is that the statistical parameters of TC wind vary with time, one may refer to Ref. [18]. Based on the potential TCI (represented by the extreme wind speed) and SLR, the parameters of the typical future scenarios can be determined.

For specific scenario, the variation of wind fields can be reconstructed to consider the landing moment and TCI effects. More specifically, the history of maximal wind speed is evaluated by multiplying the actual wind speed of typical TC in the study area (we chose the strongest TC for the study area) by the amplification coefficient firstly. Where, the amplification coefficient is determined by the maximal wind speed of assumed TCs and that of Saomai focusing on the landing moment. Subsequently, the wind fields with interval of an hour are reconstructed based on the TC wind field model. Adjusting the time coordinate of the assumed TC base on Saomai make it lands at specific moment. TC lands during astronomical high tide, the worst situation, is considered in this work. Thus, the location of the TC center can be determined. As for MSL, it can be involved by increasing the water depth of the computational domain.

Taking astronomical tide, wind and pressure fields as input, sea surface elevation can be obtained relied on the hydrodynamic model.

2.2 Hydrodynamic surge-tide-wave coupled model

The distribution and evolution of sea surface elevation can be simulated relied on the hydrodynamic model. Since surge-tide-wave coupling effects have remarkable influence on sea surface elevation.

2.2.1 Governing equations

The sea surface elevation ζ of storm tide is described by the generalized wave continuity equation (GWCE) as Eq. (1). The vertical uniform horizontal current velocity U and V are governed by the vertically-integrated momentum equations, i.e. Eqs. (2) and (3).

$$\frac{\partial^2\zeta}{\partial t^2}+\tau_0\frac{\partial\zeta}{\partial t}+S_p\frac{\partial J_\lambda}{\partial\lambda}+\frac{\partial J_\varphi}{\partial\varphi}-S_pUH\frac{\partial\tau_0}{\partial\lambda}-VH\frac{\partial\tau_0}{\partial\varphi}=0, \tag{1}$$

$$\frac{\partial U}{\partial t}+S_pU\frac{\partial U}{\partial\lambda}+V\frac{\partial U}{\partial\varphi}+\frac{\partial J_\varphi}{\partial\varphi}-fV=\frac{M_\lambda-D_\lambda}{H}-gS_p\frac{\partial}{\partial\lambda}\left(\zeta+\frac{P_S}{g\rho_0}-\alpha\eta\right)+\frac{\tau_{s\lambda,winds}+\tau_{s\lambda,waves}-\tau_{b\lambda}}{\rho_0H}, \tag{2}$$

$$\frac{\partial V}{\partial t}+S_pU\frac{\partial V}{\partial\lambda}+V\frac{\partial V}{\partial\varphi}+\frac{\partial J_\varphi}{\partial\varphi}-fU$$

$$= \frac{M_\varphi - D_\varphi}{H} - gS_p \frac{\partial}{\partial \varphi}\left(\zeta + \frac{P_S}{g\rho_0} - \alpha\eta\right) + \frac{\tau_{s\varphi,winds} + \tau_{s\varphi,waves} - \tau_{b\varphi}}{\rho_0 H}, \quad (3)$$

where λ is the longitude and φ the latitude. H is the water depth including the sea surface elevation. M_λ and M_φ are the vertically-integrated lateral stress gradients. D_λ and D_φ are the momentum dispersion terms. S_P is a spherical coordinate conversion factor. $\tau_{s\lambda,winds}$ and $\tau_{s\varphi,winds}$ are the wind stresses; $\tau_{b\lambda}$ and $\tau_{b\varphi}$ are the bottom friction stresses. g, α, ρ_0 and η are the gravitational acceleration, the tidal potential, water density and the effective earth elasticity factor, respectively. As for J_λ and J_φ, one may refer to Ref. [9].

The wave action density N is conserved during propagation in the presence of ambient current. Hence, the wind wave satisfies the balance equation of the wave action density given as

$$\frac{\partial N}{\partial t} + \frac{\partial}{\partial \lambda}[(c_\lambda + U)N] + \cos^{-1}\varphi \frac{\partial}{\partial \varphi}[(c_\varphi + V)N\cos\varphi] + \frac{\partial}{\partial \theta}[c_\theta N] + \frac{\partial}{\partial \sigma} c_\sigma N = \frac{S_{tot}}{\sigma}. \quad (4)$$

Here, c_λ and c_φ are the group velocity of wave. c_σ and c_θ are the propagation speeds in spectral space.

The aforementioned spectral wave method can account for the relevant processes of wave generation, dissipation and propagation, except diffraction. Fortunately, the influence of diffraction occurred nearshore on the water level and subsequent inundation is not significant, since waves with large amplitude have already turned into wave set-up in the surf zone and do not exist in shallow water. The source term S_{tot} is usually constituted of six processes which can be as written as Ref. (5). S_{in} is the wave energy inputted by the wind. $S_{ds,w}$, $S_{ds,b}$ and $S_{ds,br}$ are wave dissipation terms caused by white capping, bottom friction and depth-induced wave breaking, respectively. $S_{nl,3}$ and $S_{nl,4}$ represent the three-wave and four-wave interactions, respectively. For details, one may refer to Ref. [25]

$$S_{tot} = S_{in} + S_{ds,w} + S_{ds,b} + S_{ds,br} + S_{nl3} + S_{nl4}. \quad (5)$$

In this study, the ADCIRC+SWAN model developed by Dietrich et al. [9,10] is used to solve the aforementioned coupled governing equations. The continuous-Galerkin, finite-element model ADCIRC solves Eqs. (1)–(3) to obtain the time dependent sea surface elevation and current [7]. The third-generation wave model SWAN estimates the evolution of wave parameters by Eqs. (4) and (5) [26]. In every interval, ADCIRC accesses the gradients of radiation stresses by SWAN, while SWAN accesses the current and sea surface elevation provided by ADCIRC.

2.2.2 External forcing and dissipation

The hydrodynamic surge-tide-wave model described by Eqs. (1)–(5) is driven by the stresses ($\tau_{s\lambda,winds}$, $\tau_{s\varphi,winds}$, $\tau_{b\lambda}$ and $\tau_{b\varphi}$), the pressure P_s, the sea surface elevation and current of astronomic tide. They are described as follows.

$\tau_{s\lambda,winds}$ and $\tau_{s\varphi,winds}$ are determined by the drag coefficient C_d and the wind field V_{wind} at 10 m above sea surface. Here, C_d increasing linearly with wind speed as proposed by Garrat [27] is used. The wind field V_{wind} is reconstructed based on the parametric TC model given in Ref. [28], which can be decomposed into tangential wind velocity V_T, radial wind velocity V_r and environmental scale wind velocity V_E, see Eq. (6).

$$V_{wind} = V_T + V_r + V_E. \quad (6)$$

The expressions of V_T, V_r and V_E are given by Eqs. (7)–(9), respectively.

$$V_T = \frac{1}{V_m}\left(\sqrt{R^{-B}\exp(1 - R^{-B}) + a^2R^2} - aR\right), \quad (7)$$

$$V_r = \frac{B[BR^{-2B} + (1 - 3B)R^{-B} + B - 1]k - 2k - RC}{B(R^{-B} - 1) + 2 + 4aR(V_T/V_m)^{-1}} V_T, \quad (8)$$

$$V_E = U_0 \exp\left(-\frac{r}{R_G}\right). \quad (9)$$

Here, R equals to r/R_M, r the distance to the TC eye. V_m, U_0, R_G and R_M are the maximal wind velocity, the migration speed, the length scale of environmental process (of order of 500 km) and the radius of maximum wind of TC, respectively. B, C and k are coefficients, which equals to 1.5, 0.013 and 0.16, respectively. a denotes $fR_M/(2V_m)$, where f the Coriolis parameter.

The pressure field is calculated as below [28]

$$P = P_c + (P_n - P_c)\exp(-R^{-B}). \quad (10)$$

Once the maximal wind speed V_m, the central pressure P_c, the ambient pressure P_n and the track of TC are given, the wind stresses $\tau_{s\lambda,winds}$ and $\tau_{s\varphi,winds}$ and the pressure P_s can be reconstructed based on Eqs. (6)–(10).

The bottom friction stress $\tau_{b\lambda}$ ($\tau_{b\varphi}$) equals the product of density ρ_0, K_{slip} and the square of current U^2 (V^2). K_{slip} is the bottom friction coefficient given by

$$K_{slip} = C_{fmin}\left[1 + \left(\frac{H_{break}}{H}\right)^{\theta_f}\right]^{\gamma_f/\theta_f}(U + V)^{1/2}. \quad (11)$$

Here, H_{break} is the wave break depth. C_{fmin}, θ_f and γ_f are set to the recommended values, i.e. 0.0026, 10 and 1/3, respectively [29].

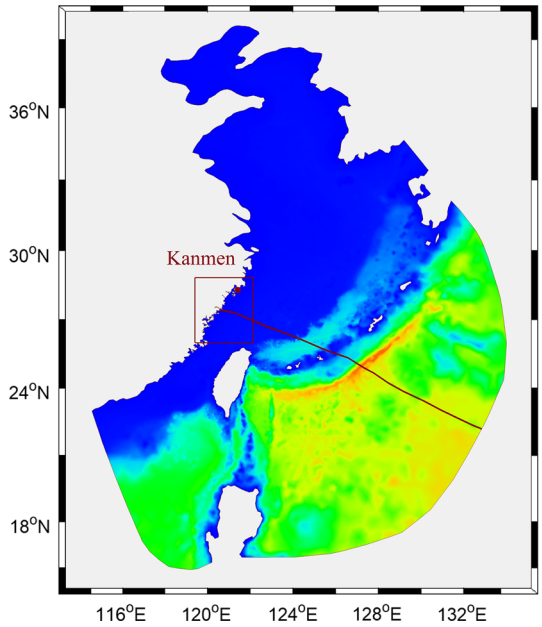

Fig. 2 Overview of the computational domain. The region by the red rectangle is the area of interest. The coordinates of the corners of the red rectangle are (119.224 ° E, 28.687 °N), (122.049 °E, 28.687 °N), (119.224 °E,25.545 °N), (122.049 °E, 25.545 °N), respectively. The red dot (28.083 °N, 121.128 °E) is the location of Kanmen tidal gauge station

Constituents from the Le Provost tidal database FES95.2 are used considering K1, K2, M2, N2, O1, P1, Q1 and S2. The tidal elevation and depth-averaged tidal current are exerted on the open boundary.

The aforementioned parameterization has been validated for TCs Thane on the India Ocean and Saomai on the Northwest Pacific Ocean. Sea surface elevation, significant wave height and surge are compared with in-situ data, and good agreements have been observed, for which one may refer to another paper of us [14].

2.3 GIS-based inundation analysis

The numerical sea surface elevation is then analyzed on the GIS platform, low-lying regions of inundation risk can be identified, and inundation hazard information including the area, inundation depth and duration for those regions can be figured out.

3 Case studies of Southeast China coast

3.1 Study area

Southeast China coast as indicated by the red rectangle in Fig. 2 is the area of interest. The whole computation domain is extended to NWP and SCS to exclude the impact of the open boundary.

The GEBCO (General Bathymetric Chart of the Oceans) bathymetry database of 30 arc second resolution is adopted. Topographic data is from the SRTM (Shuttle Radar Topography Mission) database. Unstructured grids with varying density, about 105 k elements, are adopted for the computational domain. The mesh scale at the area of interest is less than 100 m.

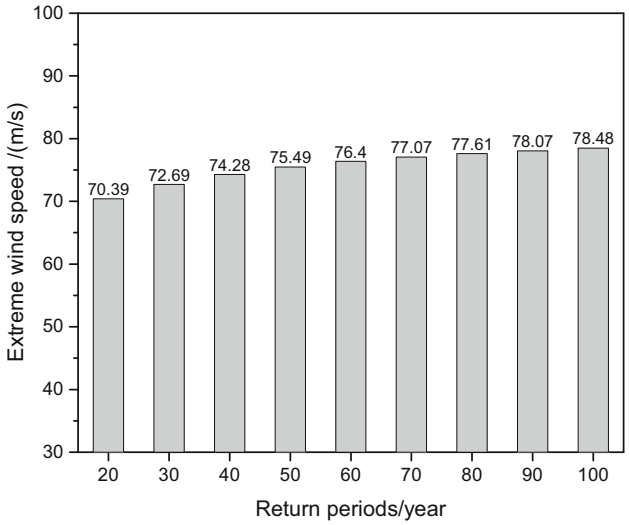

Fig. 3 Extreme wind speed of TC with different recurrence periods for the study area considering non-stationary effect

3.2 Local TCI and SLR

Relied on the non-stationary model [18], the extreme wind speeds of different recurrence periods over the study area are investigated. The main steps for estimating the extreme wind speed of TC are described as below: (1) the 72 years (1945–2013) TC database from JTWC is divided into 23 periods with 50 years in each period, i.e. 1945–1994, 1946–1995, ..., 1967–2013; (2) the shape and scale parameters of Weibull distribution for the wind speed of TC affect the area of interest are estimated for each period; (3) the time series of statistical parameters are fitted; (4) finally, the extreme wind speeds of different return periods can be obtained based on the extreme value theory as presented in Fig. 3. Taking the maximal wind speed of 50-year and 100-year recurrence period as examples, they can be as high as 75.49 m/s and 78.48 m/s, respectively.

The observed sea level series of Kanmen tidal gauge station (28.083 °N, 121.128 °E), located in the study area (see Fig. 2), is analyzed to consider the significant regional difference. It is from the Permanent Service for Mean Sea Level (PSMSL). The monthly and five-year averaged MSLs from 1959 to 2017 are presented in Fig. 4. Obvious increasing trend

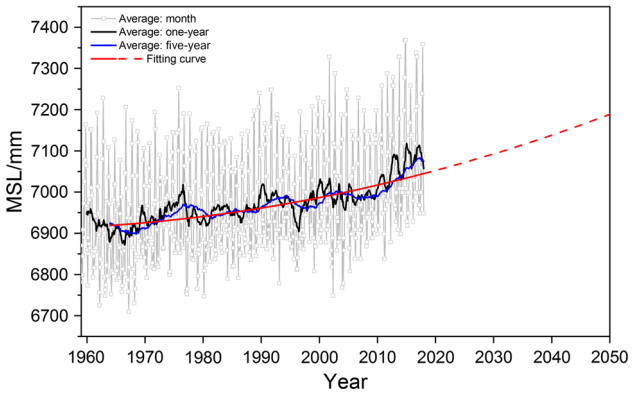

Fig. 4 MSL series of Kanmen tidal gauge station. The gray and blue solid lines are the averaged sea levels over one month and five years, respectively. The red solid line is numerical fitting result of the five-year averaged MSL, while the red-dash line is extrapolation of the fitting result

of SLR can be observed. Based on the in-situ data, numerical fitting is carried out as indicated by the red solid line in Fig. 4. The extrapolated potential SLR around 2050 is 0.185 m relative to 2006, while that around 2100 is 0.514 m. The AR5 of IPCC reported that the global SLR for 2081-2100 relative to 1986–2005 will likely be 260 to 550 mm for RCP 2.6, 320 to 630 mm for RCP 4.5, 330 to 630 mm for RCP 6.0, and 450 to 820 mm for RCP 8.5 [19]. The historical data in Kanmen gauge station shows that MSL during 1986–2005 is 6979 mm, while the extrapolation demonstrates that the local MSL during 2081–2100 would be 477 mm higher relative to 1986–2005. That is to say the SLR we obtained is between the situations of RCP 4.5 and RCP 6.0.

3.3 Scenario parameters

Examining the historical typhoons passing by the study area from 1945, it shows that Saomai has the largest wind speed during landfall. According to the National Meteorological Centre of China, the maximum wind speed of Saomai is about 60.0 m/s when landfall. Moreover, Saomai struck the coast almost vertically, the most dangerous landing angle. Therefore, it is chosen as the basic typhoon, that is S1 in Table 1. To consider the influence of astronomical tide, scenario S2 is examined in which typhoon makes landfall during the astronomical high tide. That means S2 is the worst scenario could occur at present. Then, two scenarios considering the impacts of TCI and SLR are designed based on S2. S3 has extreme wind speeds of 50-year recurrence period and SLR of 0.185 m, and S4 has extreme wind speeds of 100-year recurrence period and SLR of 0.514 m, since 50- and 100-year recurrence periods are usually considered for coastal engineering, say the national standard of China for inundation prevention at the port area in major cities. Since the variation of central pressure drop would be very likely less than 1 kPa from the present consideration (i.e. central pressure drop of Saomai, about 9 kPa when landfall) due to climate change effects, it can only bring discrepancy of sea surface level of a few centimeters, which is negligible compared with that due to strong wind shear. Therefore, the records of central pressure and track of Saomai are adopted for all the cases. The parameters for S1-S4 are provided in Table 1.

3.4 Sea surface elevation

The distributions of sea surface elevation at landing moment for scenarios S1-S4 are presented as shown in Fig. 5. It indicates that the distributions of sea surface elevation for the four scenarios are similar, but with significant difference in magnitude. Comparing S1 (see Figs. 5a) and S2 (see Fig. 5b), the landing moment has dramatic impact on the magnitude of sea surface elevation. Specifically, the maximal sea surface elevation for S2 is as high as about 5.9 m, while that for S1 is about 3.1 m. Significant difference of maximal sea surface elevation along coastline between S1 and S2 can also be observed in Fig. 7. It implies that the potential storm tide hazard if Saomai landed during the period of astronomical high tide would be much more catastrophic than the actual situation, 480 deaths and 2.5 billion USD economic loss according to the annual report of national marine hazard of 2006.

The difference of sea surface elevation between S2 and S1 linearly superposed on the tide level difference (about 4.1 m) is presented in Fig. 6. It shows that sea surface elevation of S2 can be 1.2 m (maximal) less than that of S1 linearly superposed on the tide level difference, which occurs at area north of the TC track and in the bays. While, that at most part of the computational domain is slightly larger than zero. In other words, the actual increasement of sea surface elevation due to higher tide level is less than the increasement of tide level itself, and the their relative difference can be 29% maximal. The nonlinear coupling effect between tide and surge through wave are responsible for that. More specifically, waves with larger height can survival in higher water depth, which implies wave induced surge becomes less when the astronomical tide level increases. As for the temporally evolution of sea surface elevation difference caused by the tide-surge coupling effect, Wuxi et al. [14] has shown that it will experience insignificant premonitory fluctuation, remarkable rise/drop and residual oscillating with a gentle decay of magnitude.

The maximal sea surface elevations along the coastline north of the landing location during the whole process of TC passing by for S1-S4 are plotted in Fig. 7. From Fig. 7, the curves of sea surface elevation along the coastline for S2-S4 can be divided into three segments with obvious different magnitudes of sea surface elevation, i.e. the segment 0–25 km, the segment 25–225 km and the segment beyond 225 km. The increase of sea surface elevation in the segment 0–

Table 1 Parameters of the scenarios concerned

Scenarios	MSL (mm)	TC intensity (m/s)	Central pressure	Landing moment	TC track
S1	7013.6	60.0	Saomai	Saomai	Saomai
S2	7013.6	60.0	Saomai	High tide	Saomai
S3	7198.7	75.5	Saomai	High tide	Saomai
S4	7526.6	78.5	Saomai	High tide	Saomai

Scenario S1 is the actual situation of TC Saomai. Scenario S2 is the situation that typhoon of wind speed of 100-year recurrence period makes landfall during the astronomical high tide without considering TCI and SLR. S3 (S4) corresponds to the situation that typhoon of wind speed of 50-year (100-year) recurrence period makes landfall during the astronomical high tide taking into account of the non-stationary TCI and SLR. In all the cases, the variation of central pressure and track of TCs are assumed to be same with TC Saomai

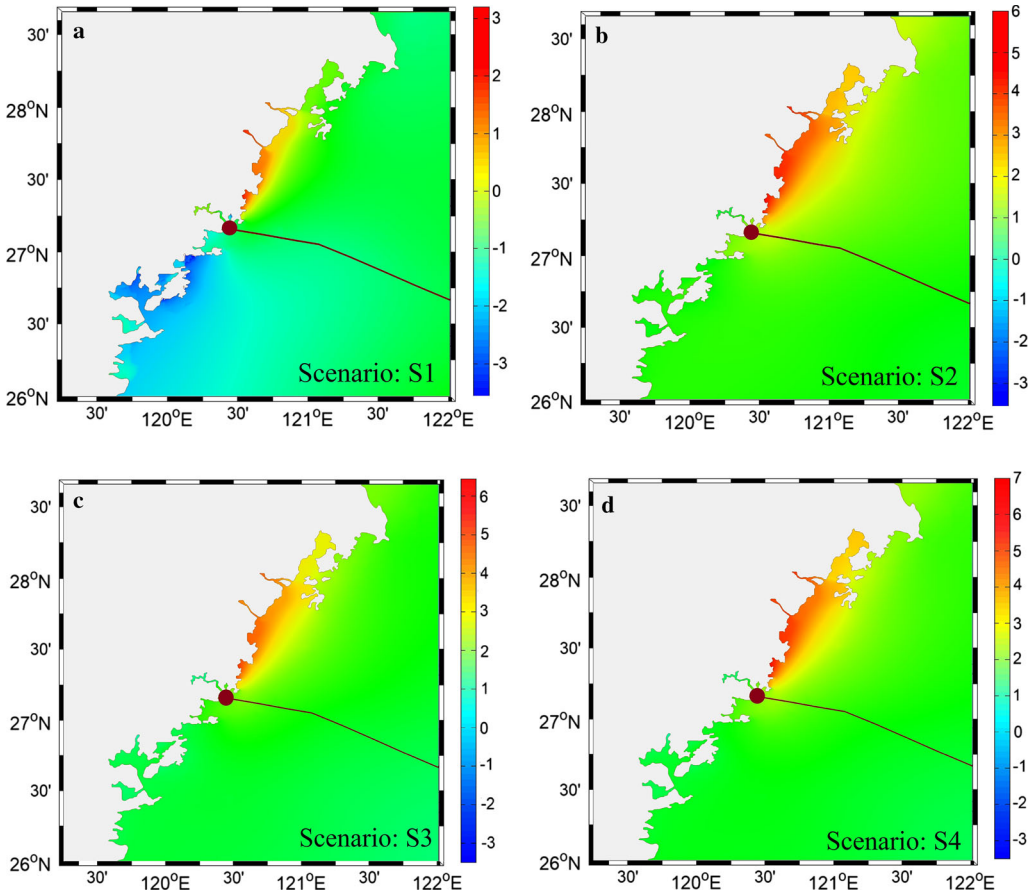

Fig. 5 Sea surface elevation (m) at landing moment. **a–d** are for secnario S1, S2, S3 and S4, respectively. The dot and line are the eye and track of TC, respectively

25 km is mainly induced by the longshore current blocked by the convex of the coastline, which occurs when the radius of maximum wind is close to the landing location. While, that in the segment 25–225 km is due to the accumulation of water body blown by wind towards coast when the eye of TC is close to the landing location. For the coastline out of the radius of maximal wind, i.e. the segment beyond 225 km, sea surface elevation is much smaller owing to weaker wind shear. Figure 7 shows that the average maximal sea surface elevations along the coastline 0–275 km are 4.91 m, 5.25 m and 5.71 m for S2-S4, respectively.

On the other hand, the assessment of the warning water level for storm-surge-prevention issued by Zhejiang Province in 2016 demonstrates that the red (highest level) warning water level is only about 4.25–4.65 m over the MSL for this region. Where, the red warning water level at the coastal region with seawall is computed by the lowest seawall with a small correction value (< 1–20 cm) considering factors including wave runup, type and important level of the sea-

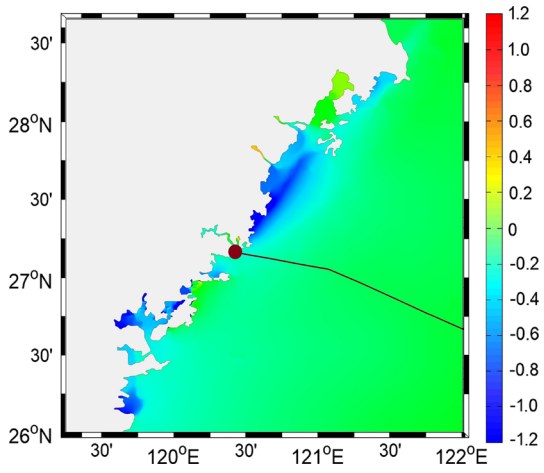

Fig. 6 Difference of sea surface elevation (m) between S2 and S1 with the astronomical tide excluded

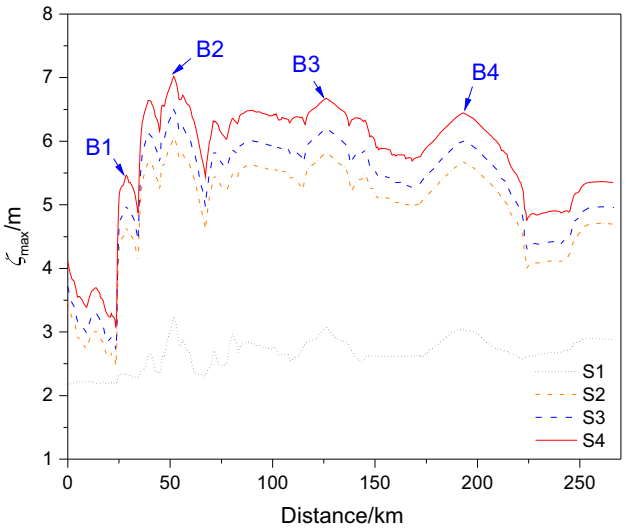

Fig. 7 Maximal sea surface elevation along the coastline during the whole process of TC landing. B1–B4 are the extremums of sea surface elevation with their locations marked in Fig. 8. The horizontal axis represents the distance to the landing location of the TC eye

wall. That means the existing seawall would be overtopped severely, and they can only affact the intrusion flow and inundation locally and instantaneously due to its small size compared with the backward intrusive distance. Moverover, a few hundred kilometres of seawall damaged in a single intermediately strong storm surge is quite common according to the Annual Report of National Marine Hazard of China, hence, the efficiency of seawall there will decreses further. Therefore, adquate planning of future urbanization shall be carried out based on corresponding risk analysis taking into climate change into account in addition to strengthening the sea wall.

The comparison between S2 and S4 (S3) indicates that the non-stationary TCI and SLR effects increase sea surface elevation by 0.80 m (0.34 m) on average for the coastline concerned. Accordingly, we can conclude that sea surface elevation will be underestimated remarkably without considering the climate change impact (TCI and SLR).

Since the period of astronomical tide cycle is a few times larger than the duration of TC passing by for a specific location, the increase of tide level can be regarded as the quasi-steady process of increasing the water depth. That is similar to SLR, but much larger amplitude. It implies that the increasement of sea surface elevation contributed by SLR can be estimated roughly by the tide-surge coupling effect. Taking S4 for example. The MSL of S4 is 0.51 m higher than that of S2. That means increase of sea surface elevation caused by SLR will be a little bit less than 0.51 m, because less wave induced surge occurs for higher water depth. While, the total increase of sea surface elevation by SLR and TCI, 0.80 m, suggests that increase of sea surface elevation caused by TCI could be larger than 0.29 m. The qualitative results can be obtained for S3 similarly, i.e. TCI could cause more than 0.16 m of sea surface elevation increasement, while SLR can caused sea surface elevation increasement a little bit less than 0.19 m. In all, both TCI and SLR are important factors should be involved in the future long-term hazard assessment of storm tide.

Further, the locations of the extremums of sea surface elevation curves in Fig. 7, i.e. B1–B4, are marked in Fig. 8. It demonstrates that high sea surface elevation occurs in the bays or at the river estuaries, since water body is easy to accumulate in such geography. Specifically, B1 is the bay near the landing location of the TC eye; while B2–B4 are Aojiang river estuary, Feiyunjiang river estuary and Oujiang river estuary, respectively. The maximal sea surface elevations at Aojiang river estuary are 6.06 m, 6.51 m and 7.02 m for S2–S4, respectively. While the maximal sea surface elevations at Feiyunjiang river estuary are 5.82 m (S2), 6.20 m (S3) and 6.67 m (S4), respectively, and that at Oujiang river estuary are 5.67 m (S2), 6.00 m (S3) and 6.44 m (S4), respectively.

3.5 Inundation

Relied on the inundation model of GIS platform, the potential inundation regions with area larger than 10 km^2 for S2 and S4 are identified as shown in Figs. 8 and 9, respectively. From Fig. 8, the south coast of Aojiang river (R2), the south coast of Oujiang river (R5), the alluvial island at Oujiang river estuary (R6) and the north coast of Oujiang river (R7) are the largest four regions inundated. And low-lying regions R1 and R8 are also under the threat of inundation. As for S4 with the non-stationary TCI and SLR effects considered, the aforementioned six regions enlarge significantly. In addition, the north coast of Aojiang river (R3), the south and north coasts

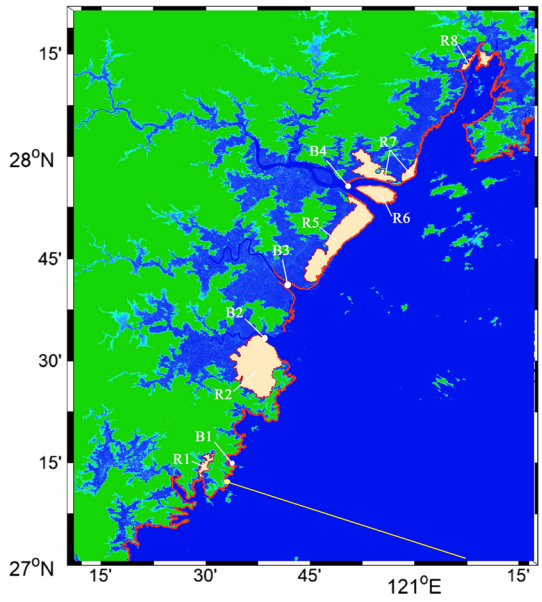

Fig. 8 Overview of the potential inundation regions for S2. The red lines are the boundaries of the inundation regions. Polygons marked as R1, R2 and R5–R8 are six regions with severe inundation hazard identified. The typhoon track and land location are sketched by the yellow solid line with a dot at the end. B1–B4 are the locations of the extremums of sea surface elevation in Fig. 7

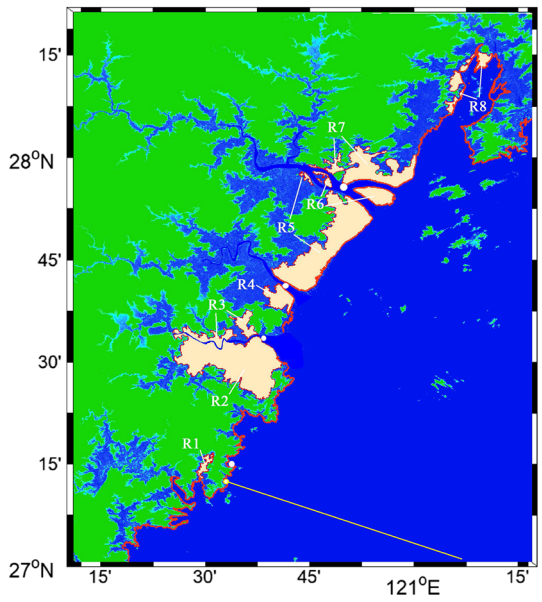

Fig. 9 Overview of the potential inundation regions for S4. The red lines are the boundaries of the inundation regions. Polygons marked as R1–R8 are eight regions with severe inundation hazard identified. The typhoon track and land location are sketched by the yellow solid line with a dot at the end

of Feiyunjiang river (R4 and R5) expose to the storm tide as well. The areas of the aforementioned inundation regions are presented in Table 2, and the lengths of the coastlines where water body intruded are also presented along with. From Table 2, about 379 km^2 is under the threat of storm tide inundation for S2. As for S4, the potential inundation will increase by 108% to about 798 km^2. That is to say, the storm tide inundation area will be underestimated remarkably as well without considering the non-stationary TCI and SLR effects.

Table 2 shows that the estuaries of Aojiang river (B2), Feiyunjiang river (B3) and Oujiang river (B4) are the hardest hit regions. The remotely sensed maps of the three hardest hit regions are presented in Fig. 10. The coastlines where water intruded are sketched by white solid lines, the farthest boundary of water body intruded for scenarios S2 and S4 are marked by red and blue lines, respectively. Figure 10a shows that the Cangnan city located at the south coast of Aojiang river is suffering from storm tide inundation hazard for S2 partly. As for S4, the whole downtown of Cangnan city and almost half of Aojiang town located at the north coast of Aojiang river are exposed to the storm tide inundation. At the estuary of Feiyunjiang river (see Fig. 10b), most of the inundation areas are farmland. Figure 10c shows that most of the Longwan and Dongtou districts of Wenzhou city are of high risks of storm tide inundation.

To provide reference for the local vulnerability assessments, the mean inundation durations for spots with different heights over MSL for S2–S4 are also provided in Fig. 11 roughly. It shows that the inundation duration of S4 ranks the first followed by S3 and S2, which is consistent with their sea surface elevations. Form Fig. 11, the inundation duration is not spatial homogeneous, and the estuary of Feiyunjiang river experiences longer period than the other two estuaries. It is noteworthy that the actual inundation duration can be adjusted by the protective constructions such as sea walls. For example, the actual inundation duration of S4 could maintain longer than the duration predicted, especially for the spots lower than the sea wall, because sea wall was already overtopped severely and the water swarmed into will be blocked when the sea surface level gradually decreases after landfall of TC.

4 Conclusions

Storm tide is the deadliest marine hazard, which has claimed large numbers of human lives and shocking economic losses. With the evidences of rapid global warming, say temperature at Antarctic breaks the record recently, the potential storm tide inundation is by no means optimistic due to TCI and SLR. Case studies of storm tide inundation under TCI and SLR along Southeast China coast, one of the storm surge prone areas in China, are carried out. The specific procedures are: (1) analyzing the the long-term historical database of the study area, the tropical cyclone intensification (TCI) and sea level rise (SLR) considering temporally non-stationary and spatially non-uniform effects can be obtained; (2) sea surface

Table 2 Area and length of the coastlines where water body intruded for the inundation regions

Scenarios		R1	R2	R3	R4	R5	R6	R7	R8	Total
S2	Area (km^2)	10.2	144.7	0	0	122.1	30.5	54.6	17.1	379.2
	Length (km)	1.6	13.9	0	0	32.8	25.3	15.5	17.8	106.9
S4	Area (km^2)	10.2	273.9	47.0	35.3	235.0	37.6	117.8	41.5	789.3
	Length (km)	1.9	13.9	3.3	10.5	53.9	32.6	25.8	30.0	171.9

Fig. 10 Remotely sensed maps of hardest hit regions of storm tide inundation. Plots **a**, **b** and **c** are for the estuaries of Aojiang river, Feiyunjiang river and Oujiang river, respectively. The white line indicates the coastline where water body intruded. The red and blue lines correspond to the inundation lines for S2 and S4, respectively. Source ©Google Earth

elevations of typical potential storm tide scenarios is simulated using the ADCIRC+SWAN model to take into account the tide-surge-wave coupling effect for better precision; (3) the potential inundated regions are identified relied on the GIS platform.

The results demonstrate that the bays and estuaries in this coastal area tend to experience more dramatic rising process

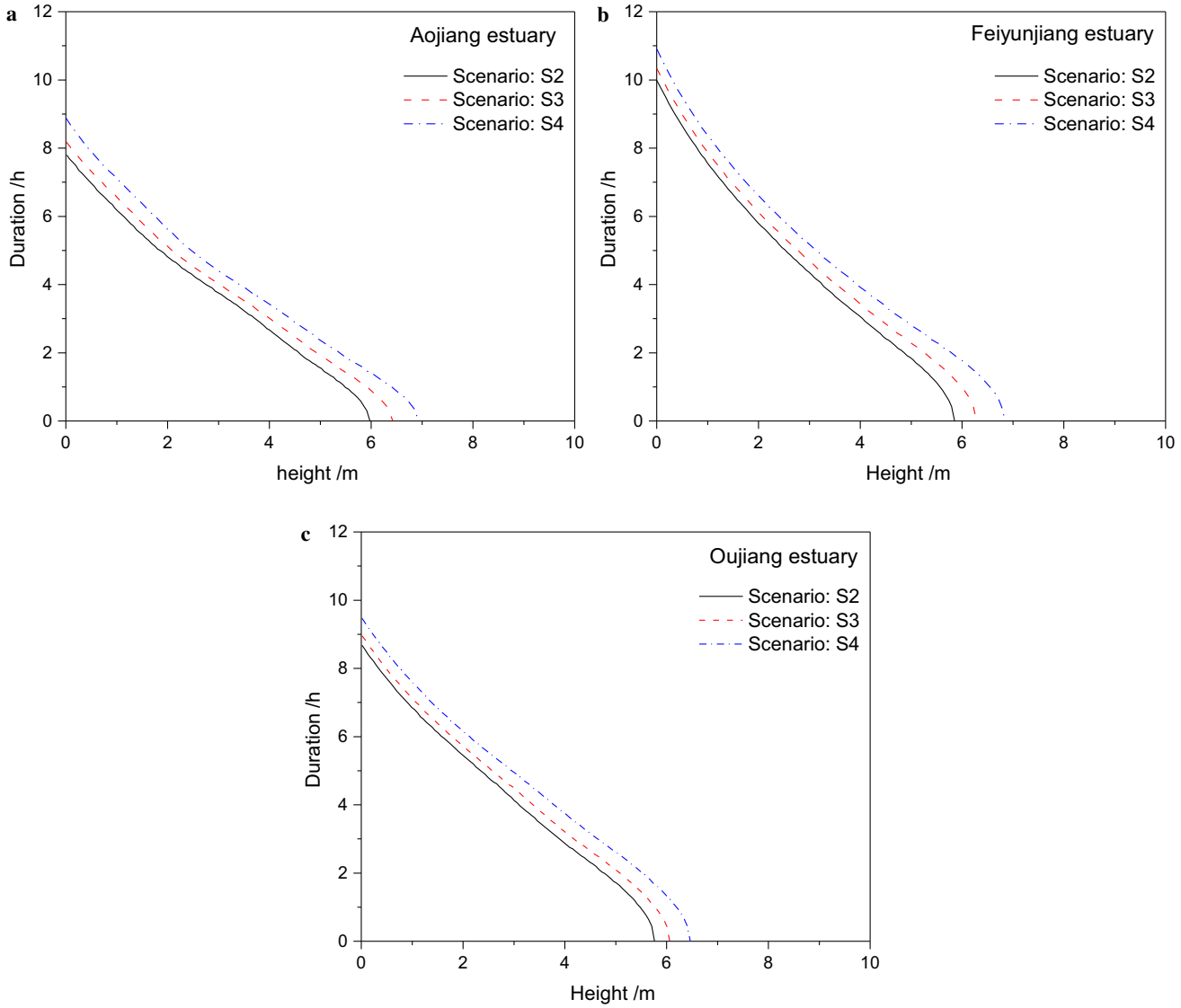

Fig. 11 Inundation duration for the hardest hit regions of storm tide inundation without considering the protective constructions such as sea walls. Plots **a**, **b** and **c** are for the estuaries of Aojiang river, Feiyunjiang river and Oujiang river, respectively. The horizontal axis represents the height over the MSL. The solid line, dash line and dot dash line are for scenarios S2, S3 and S4, respectively

of sea surface elevation. As for the worst situation at present without consider SLR and TCI (i.e. scenario S2), the maximal sea surface elevation around the estuary of Aojiang river can be 6.06 m, while that around the Feiyunjiang and Oujiang river estuaries can be 5.82 m and 5.67 m, respectively. Under this circumstances, roughly 379 km^2 of coast area is under the threat of storm tide inundation.

Non-stationary TCI and SLR have remarkable impacts on the storm tide elevation and subsequent inundation. The sea surface elevations of two scenarios are provided, i.e. Scenario S3 of extreme wind speeds of 50-year recurrence period and corresponding SLR of 0.185 m, and scenario S4 of extreme wind speeds of 100-year recurrence period and corresponding SLR of 0.514 m. The maximal sea surface elevations of S4 can be as high as 7.02 m (Aojiang river estuary), 6.67 m (Feiyunjiang river estuary) and 6.44 m (Oujiang river estuary). While that for S3 are 6.51 m, 6.20 m and 6.00 m, respectively. Both are much higher than that of S2 and the red (highest level) warning water level issued by the government for storm-surge-prevention there (4.3–4.6 m maixmal). The corresponding potential inundated area of S4 could expand by 108% to about 798 km^2 comparing with S2.

The remotely sensed maps for the most heavily hit regions of S4, i.e. the estuaries of Aojiang, Feiyunjiang and Oujiang rivers are provided as well, which demonstrate that a few number of downtowns such as Cangnan city and Wenzhou city are exposed to the threat of storm tide inundation.

In conclusion, the factors owing to climate change can be no longer neglected in the future risk assessment of storm tide disasters. In addition, real-time topography considering urbanization and protective constructions such as sea walls, relevant social and economic data are expected to be integrated in the present study for risk assessment of high precision.

Acknowledgements This work is supported by the National Natural Science Foundation of China (Grant 11902024), the National Key R&D Program of China (Grant 2017YFC1404202), and the Strategic Priority Research Programs (Category B) of the Chinese Academy of Sciences (Grant XDB22040203). The authors also thank Dr. Guoqin Lyu for the assistance with the non-stationary estimation of extreme wind speed of TC.

References

1. Li, J.C., Nie, B.C.: Storm surge prediction: present status and future challenges. Proc. IUTAM **25**, 3–9 (2017). https://doi.org/10.1016/j.piutam.2017.09.002
2. Lagmay, A.M.F., Agaton, R.P., Bahala, M.A.C., et al.: Devastating storm surges of Typhoon Haiyan. Int. J. Disast. Risk Re. **11**, 1–12 (2015). https://doi.org/10.1016/j.ijdrr.2014.10.006
3. Hsu, C.H., Olivera, F., Irish, J.L.: A hurricane surge risk assessment framework using the joint probability method and surge response functions. Nat. Hazards **91**, S7–S28 (2018). https://doi.org/10.1007/s11069-017-3108-8
4. Christie, E.K., Spencer, T., Owen, D., et al.: Regional coastal flood risk assessment for a tidally dominant, natural coastal setting: North Norfolk, southern North Sea. Coast. Eng. **134**, 177–190 (2018). https://doi.org/10.1016/j.coastaleng.2017.05.003
5. Younus, M.A.F.: An assessment of vulnerability and adaptation to cyclones through impact assessment guidelines: a bottom-up case study from Bangladesh coast. Nat. Hazards **89**, 1437–1459 (2017). https://doi.org/10.1007/s11069-017-3027-8
6. Taflanidis, A.A., Kennedy, A.B., Westerink, J.J., et al.: Rapid assessment of wave and surge risk during landfalling hurricanes: probabilistic approach. J. Waterw. Port C. **139**, 171–182 (2013). https://doi.org/10.1061/(ASCE)WW.1943-5460.0000178
7. Jelesnianski, C.P., Chen, J., Shaffer, W.A.: SLOSH: sea, lake, and overland surges from hurricanes, NOAA Technical Report. NWS **48**, (1992)
8. Luettich, R.A.J., Westerink, J.J., Scheffner, N.W.: ADCIRC: an advanced three dimensional circulation model for shelves, coasts and estuaries. Report 1: theory and methodology of ADCIRC-2DDI and ADCIRC-3DL, Technical Report DRP-92-6 (1992)
9. Dietrich, J.C., Zijlema, M., Westerink, J.J., et al.: Modeling hurricane waves and storm surge using integrally-coupled, scalable computations. Coast. Eng. **58**, 45–65 (2011). https://doi.org/10.1016/j.coastaleng.2010.08.001
10. Dietrich, J.C., Tanaka, S., Westerink, J.J., et al.: Performance of the unstructured-mesh, SWAN+ADCIRC model in computing hurricane waves and surges. J. Sci. Comput. **52**, 468–497 (2012). https://doi.org/10.1007/s10915-011-9555-6
11. Wu, L., Chen, C.S., Guo, P.F., et al.: A FVCOM-based unstructured grid wave, current, sediment transport model, I Model description and validation. J. Ocean U. China **10**, 1–8 (2011). https://doi.org/10.1007/s11802-011-1788-3
12. Roland, A., Zhang, Y.J., Wang, H.V., et al.: A fully coupled 3D wave-current interaction model on unstructured grids. J. Geophys. Res. Oceans **117**, C00J33 (2012) https://doi.org/10.1029/2012JC007952
13. Zhang, H., Cheng, W.C., Qiu, X.X., et al.: Tide-surge interaction along the east coast of the Leizhou Penunsula, South China Sea. Cont. Shelf Res. **142**, 32–49 (2017). https://doi.org/10.1016/j.csr.2017.05.015
14. Wuxi, Q.Y., Li, J.C., Nie, B.C.: Effects of tide-surge interaction and wave set-up/set-down on surge: case studies of tropical cyclones landing China's Zhe-Min coast. Theor. Appl. Mec. Lett. **8**, 153–159 (2018). https://doi.org/10.1016/j.taml.2018.03.002
15. Webster, P.J., Holland, G.J., Curry, J.A., et al.: Changes in tropical cyclone number, duration, and intensity in a warming environment. Science **309**, 1844–1846 (2005). https://doi.org/10.1126/science.1116448
16. Elsner, J.B., Kossin, J.P., Jagger, T.H.: The increasing intensity of the strongest tropical cyclones. Nature **455**, 92–95 (2008). https://doi.org/10.1038/nature07234
17. Knutson, T.R., McBride, J.L., Chan, J., et al.: Tropical cyclones and climate change. Nat. Geosci. **3**, 157–163 (2010). https://doi.org/10.1038/ngeo779
18. Wang, L.Z., Li, J.C.: Estimation of extreme wind speed in SCS and NWP by a non-stationary model. Theor. Appl. Mec. Lett. **6**, 131–138 (2016). https://doi.org/10.1016/j.taml.2016.04.001
19. IPCC: Climate change 2014 synthesis report, Contribution of Working Group III to the Fifth Assessment Report of the Intergovernmental Panel on Climate Change (2015)
20. Feng, X.R., Li, M.J., Yin, B.S., et al.: Study of storm surge trends in typhoon-prone coastal areas based on observations and surge-wave coupled simulations. Int. J. Appl. Earth Obs. **68**, 272–278 (2018). https://doi.org/10.1016/j.jag.2018.01.006
21. Wang, J., Gao, W., Xu, S.Y., et al.: Evaluation of the combined risk of sea level rise, land subsidence, and storm surges on the coastal areas of Shanghai, China. Clim. Change **115**, 537–558 (2012). https://doi.org/10.1007/s10584-012-0468-7
22. Feng, A.Q., Gao, J.B., Wu, S.H., et al.: Assessing the inundation risk resulting from extreme water levels under sea-level rise: a case study of Rongcheng, China. Geomat. Nat. Haz. Risk **9**, 456–470 (2018). https://doi.org/10.1080/19475705.2018.1447026
23. Yin, K., Xu, S.D., Huang, W.R., et al.: Effects of sea level rise and typhoon intensity on storm surge and waves in Pearl River Estuary. Ocean Eng. **136**, 80–93 (2017). https://doi.org/10.1016/j.oceaneng.2017.03.016
24. Li, N., Yamazaki, Y., Roeber, V., et al.: Probabilistic mapping of storm-induced coastal inundation for climate change adaptation. Coast. Eng. **133**, 126–141 (2018). https://doi.org/10.1016/j.coastaleng.2017.12.013
25. Zijema, M.: Computation of wind-wave spectra in coastal waters with SWAN on unstructured grids. Coast. Eng. **57**, 267–277 (2010). https://doi.org/10.1016/j.coastaleng.2009.10.011
26. Booij, N., Ris, R.C., Holthuijsen, L.H.: A third-generation wave model for coastal regions, 1. Model description and validation. J. Geophys. Res. Oceans **104**, 7649–7666 (1999). https://doi.org/10.1029/98JC02622
27. Garrat, J.R.: Review of drag coefficients over oceans and continents. Mon. Weather Rev. **105**, 915–929 (1977)
28. Jakobsen, F., Madsen, H.: Comparison and further development of parametric tropical cyclone models for storm surge modelling. J. Wind Eng. Ind. Aerod. **92**, 375–391 (2004). https://doi.org/10.1016/j.jweia.2004.01.003
29. Luettich, R.A., Westerink, J.J.: ADCIRC: A (parallel) advanced circulation model for oceanic, coastal and estuarine waters, user's manual for version 51 (2006)

Publisher's Note Springer Nature remains neutral with regard to jurisdictional claims in published maps and institutional affiliations.